JAERI-M
88-179

MODULE TYPE FLAT-FIELD GRAZING INCIDENCE SPECTROGRAPHS FOR LARGE TOKAMAK (JT-60) PLASMA DIAGNOSIS : DESIGN AND IMAGING PROPERTIES

September 1988

Hiroshi NAGATA*, Makoto SHIHO and Tatsuo SUGIE

日本原子力研究所
Japan Atomic Energy Research Institute

JAERI-M レポートは，日本原子力研究所が不定期に公刊している研究報告書です。
入手の問合わせは，日本原子力研究所技術情報部情報資料課（〒319-11茨城県那珂郡東海村）あて，お申しこしください。なお，このほかに財団法人原子力弘済会資料センター（〒319-11 茨城県那珂郡東海村日本原子力研究所内）で複写による実費頒布をおこなっております。

JAERI-M reports are issued irregularly.
Inquiries about availability of the reports should be addressed to Information Division Department of Technical Information, Japan Atomic Energy Research Institute, Tokai-mura, Naka-gun, Ibaraki-ken 319-11, Japan.

編集兼発行　日本原子力研究所
印　　刷　㈱高野高速印刷

Module Type Flat-Field Grazing Incidence Spectrographs for large TOKAMAK (JT-60) Plasma Diagnosis: Design and Imaging Properties

Hiroshi NACATA*, Makoto SHIHO+ and Tatsuo SUGIE

Department of Large Tokamak Research
Naka Fusion Research Establishment
Japan Atomic Energy Research Institute
Naka-machi, Naka-gun, Ibaraki-ken

(Received August 31, 1988)

Module type flat-field grazing incidence spectrographs equipped with holographic grating are designed for the impurity diagnosis of large TOKAMAK (JT-60) plasma in the wavelength region of 0.5-122 nm. The spectrographs are with common size, and they cover different wavelength regions by changing the grating. The design requirement and characteristics of the spectrographs are summarized. Optical design and designed properties are discussed. The preliminary tests with photographic plates are examined, and many spectra including Al Kα (0.83 nm) are recorded. These spectrographs show the designed flat-field character, and sufficient wavelength resolution for plasma diagnosis.

Keywords: Flat-Field, Grazing Incidence Spectrograph, Tokamak, JT-60, Diagnostics, Holographic Grating

+ Department of Thermonuclear Fusion Research
* Nikon Corporation.

ＪＴ－６０トカマクプラズマ診断用
平面結像型斜入射分光器：設計と結像特性の評価

日本原子力研究所那珂研究所臨界プラズマ研究部
永田　浩*・志甫　諒+・杉江達夫

（１９８８年８月３１日受理）

大型トカマク装置ＪＴ－６０の不純物計測用に，ホログラフィック回折格子を使ったモジュール型平面結像斜入射分光器を0.５－１２２ｎｍの波長範囲で設計した。このモジュール型分光器は非常にコンパクトであり，回折格子を変え，検出器の位置をほんの少しだけ動かすことにより，異なった波長範囲を測定できる。また，Ａ１Ｋα（0.８３ｎｍ）線等のスペクトル線を発光する軟Ｘ線域の光源を使い，この分光器を試験した結果，平面結像性・分解能等，設計どうりの性能が確認された。

那珂研究所：〒３１１－０１　茨城県那珂郡那珂町大字向山８０１－１
＋　核融合研究部
＊　（株）ニコン

Contents

目　　次

1. Introduction

During the last decade, various aberration-corrected gratings have been designed and produced both by recording interference fringes in photoresist and by using numerically controlled ruling engines in order to develop new types of spectroscopic instruments.[1-9] Among these, a grating for a flat-field spectrograph is very attractive in that its flat focal plane facilitates the use of an array detector for simultaneous photoelectric detection of a spectrum over a wide wavelength region.[4-9] Flat-field spectrographs are useful in plasma diagnosis, i.e., in real-time measurement and control of plasmas. Fonck et al. developed a spectrograph equipped with toroidal holographic gratings for diagnosis of PDX TOKAMAK plasmas in the 10-170 nm wavelength region.[6,9] Kita et al. took spectra of laser-produced plasmas in the 5-20 nm wavelength region with a flat-field spectrograph equipped with a mechanically ruled grating,[7] and later they succeeded in going down to 1.5 nm with a finer grating.[8]

For the impurity diagnosis of large TOKAMAK(JT-60) plasma, space-resolved simultaneous intensity measurements are essentially important. The design requirements of the spectrographs are as follows;

I. wavelength region is 0.5-122 nm,
II. wavelength resolution $\lambda/d\lambda$ is equivalent to conventional Rowland circle monochromator (10 at 0.5 nm, 100 at 5 nm, 300 at 20 nm),
III. spatial resolution is 7 cm,
IV. time resolution is 20 ms,
V. easy to install, to exchange, and to repair.

We developed module type flat-field grazing incidence spectrographs with holographic grating which satisfy these requirements. These spectrographs coupled with photo-electric array detector are working now, and some results are reported.[10-12] In this paper, we describe the basic considerations for these spectrographs, including the design characteristics, the detailed design procedure, and the expected performance of the spectrographs. The results of the preliminary tests with photographic plates are also shown.

2. Summarization of the design characteristics

Considering the requirements described in Sec. 1, we designed four spectrographs for JT-60 plasma diagnosis which have following characteristics;

1. Introduction

During the last decade, various aberration-corrected gratings have been designed and produced both by recording interference fringes in photoresist and by using numerically controlled ruling engines in order to develop new types of spectroscopic instruments.[1-9] Among these, a grating for a flat-field spectrograph is very attractive in that its flat focal plane facilitates the use of an array detector for simultaneous photoelectric detection of a spectrum over a wide wavelength region.[4-9] Flat-field spectrographs are useful in plasma diagnosis, i.e., in real-time measurement and control of plasmas. Fonck et al. developed a spectrograph equipped with toroidal holographic gratings for diagnosis of PDX TOKAMAK plasmas in the 10-170 nm wavelength region.[6,9] Kita et al. took spectra of laser-produced plasmas in the 5-20 nm wavelength region with a flat-field spectrograph equipped with a mechanically ruled grating,[7] and later they succeeded in going down to 1.5 nm with a finer grating.[8]

For the impurity diagnosis of large TOKAMAK(JT-60) plasma, space-resolved simultaneous intensity measurements are essentially important. The design requirements of the spectrographs are as follows;

I. wavelength region is 0.5-122 nm,
II. wavelength resolution $\lambda/d\lambda$ is equivalent to conventional Rowland circle monochromator (10 at 0.5 nm, 100 at 5 nm, 300 at 20 nm),
III. spatial resolution is 7 cm,
IV. time resolution is 20 ms,
V. easy to install, to exchange, and to repair.

We developed module type flat-field grazing incidence spectrographs with holographic grating which satisfy these requirements. These spectrographs coupled with photo-electric array detector are working now, and some results are reported.[10-12] In this paper, we describe the basic considerations for these spectrographs, including the design characteristics, the detailed design procedure, and the expected performance of the spectrographs. The results of the preliminary tests with photographic plates are also shown.

2. Summarization of the design characteristics

Considering the requirements described in Sec. 1, we designed four spectrographs for JT-60 plasma diagnosis which have following characteristics;

A. the size of the spectrographs is common, 670 mm(l) × 150mm(w) × 60 mm(h),
B. positions of the entrance slit and the grating are fixed, and that of the focal plane is almost invariant,
C. by changing the grating, each spectrograph covers certain wavelength region, 0.5-5 nm, 0.5-50 nm, 2-50 nm, and 50-122 nm, respectively (we call these spectrographs as S1, S2, S3, and S4),
D. incident angles of the spectrographs are 89° for S1 and S2, 88° for S3, and 85° for S4,
E. image plane is flat, the incident angle of the diffracted ray to the image plane is smaller than 30°, and the length of the image plane is fit to the commercially available array detector,
F. wavelength resolution $\lambda/d\lambda$ is better than 150 at 5 nm with photographic plate, and equivalent to conventional Rowland circle monochromator with photo-electric detector,
G. a vacuum vessel with seventeen guide bars is prepared, and the modularized spectrographs are inserted along the guide bars,
H. each modularized spectrograph observes different spatial position of the plasma, and realizes the spatial resolution of 7 cm.

The flat-field grazing incidence spectrogrphs with the photo-electric detector are suitable for measuring requirements I, II and IV. Moreover, when these spectrographs are modularized and inserted along the guide bar in the vacuum vessel, they also satisfy the other requirements III and V. The schematic diagram of the modularized spectrograph is shown in Fig. 1, and the arrangement of the spectrographs for space resolved large TOKAMAK plasma diagnosis is shown in Fig. 2. The merits of the instrument (the modularized spectrographs and the vaccum vessel) are as follows;

(1) handling of the spectrographs is easy, and needs no skill,
(2) the vacuum vessel is connected to JT-60 TOKAMAK and fixed, and free from putting on and taking off the spectrograph,
(3) measuring wavelength region or ther spectrscopic conditions can be changed easily by changing the modularized spectrograph,
(4) even by changing the spectrograph, the optical axis through the plasma does not move,
(5) adjustment of the spectrograph can be done at a different place apart from JT-60 TOKAMAK.

Other design considerations which satisfy the requirements I-V and bring the characteristics A-H are described below.

a) Spatial region and wavelength region to be measured

The vacuum vessel of JT-60 TOKAMAK is a doughnut type, its major radius is 3 m, and the minor radius, the radius of the cross section, is 1 m. The spatial distribution of the impurities changes along the minor radius, and the upper half area of the plasma cross section is measured by dividing into 15 measuring chords. (this situation is already shown in Fig. 2) The required spatial resolution is 7 cm at the plasma, which is discussed in detail in Sec. 3.

The wavelength region to be measured is 0.5-122 nm. For the wavelength region shorter than 0.5 nm, crystal spectrometers are prepared, and the longest wavelength to be measured is Hydrogen L α (121.6 nm). To cover this wavelength region, two spectrographs, S2 and S4, which cover 0.5-50 nm and 50-122 nm respectively, are considered. In this case, however, the wavelength resolution of S2 becomes poor in the wavelength region shorter than 5 nm. Thus another spectrograph S1 which covers 0.5-5 nm with higher resolution is added. One more spectrograph S3, covers 2-50 nm, is also designed. The wavelength region of S3 is overlapped with that of S2, but with different incident angles.

b) Size of the spectrograph

The size of the modularized spectrograph is limited by the following requirements: (1) the module should be compact, easy to hold by hand, (2) the space permitted for the vacuum vessel of the spectrograph is restricted from the construction around the JT-60, (3) the module can be put on and taken off without interference with other instruments and surrounding wall, (4) the designed condition for the production of the gratings can be realized, (5) the resolution and the length of the image plane of the spectrograph should match the detector, (6) the distances among components of the spectrograph are suitable to assemble.

From the requirements (1)-(3), the upper boundary of the size of the modularized spectrograph is determined as 750 mm(l) × 160 mm(w) × 60 mm(h). Considering the length of the detector and the space between the edge of the module and the entrance slit, the upper boundary of the distance from the entrance slit to the image plane is about 550 mm. From the requirements (4)-(6), the lower boundary is determined. This value depends on the designed results which is described below, they show the lower boundary of the distance from the entrance slit to the image plane is about 400 mm.

c) Incident angle

The incident angle of the spectrograph for soft X-ray region is determined by the reflectance of the grating material at the shortest wavelength to be measured. Here, Pt is assumed as the grating surface material, and the reflectance of more than 50% is considered. The calculated reflectance from the optical constants[13,14] is 69% at the wavelength of 0.6 nm and the incident angle of 89°, 64% at 2 nm and 88°, and 69% at 50 nm and 80°. Thus the incident angles are determined as 89° for S1 and S2, and 88°for S3. For S4, the maximum width of the modularized spectrograph is restricted from the narrow space for the instruments, the incident angle of 85° is adopted.

The incident angles of the modularized spectrographs are different, but the directions of the optical axes are invariant.

d) Detector

The detector for this spectrograph is required to be a multi-channel detector with high sensitivity in VUV wavelength region. For this requirement, one dimensional array detector coupled with MCP as a face plate is considered. For example, a detector which has an array sensor of 1024 or 2048 channels with 25 μm channel pitch is commercially available.

The spatial resolution of the detector is deteriorated by the spread of the electron flux and electron-photon conversion in the detector, it is estimated about 50 μm. The sensitivity of MCP changes with the incident angle of the light on it. For the grazing angle, it goes down more than 2 orders of magnitude as compared to the maximum value. To prevent this decrease in the sensitivity, the incident angle of the diffracted ray to the detector is restricted to smaller than 30°.

The period of the data acquisition is 20 ms, which corresponds to the integration time of the light flux on the detector.

e) Wavelength resolution

For the impurity measurement, the required data is the intensity of the known spectra. The detailed line profile measurement of the spectra and identification of the spectra are done with another instrument. Thus the wavelength resolution which is equivalent to conventional Rowland circle monochromator used for JFT-2 plasma is taken as a reference. The values of $\lambda/d\lambda$ in that case were 10 at 0.5 nm, 100 at 5 nm, and 300 at 20 nm (these values are the results with wide slit width because of weak light intensity). The resolution of the spectrograph is restricted with a slit width, residual aberrations, and the detector. In our design, the

resolution of the detector is dominant, which is discussed later.

3. Optical design and optical performance

3.1 Design procedure

The optimum image plane is determined in two steps. Firstly, the light path function of the spectrograph is expanded and coefficients of lower orders are minimized, then an approximate solution is determined. Secondly, from this solution, optimum one is determined by ray tracing, where the density of sports in the image plane at several wavelengths is chosen as the merit function.

We refer to Fig. 3 to describe our procedure of designing a concave holographic grating (H.G.) with a radius R for a flat-field spectrograph. We introduce a rectangular coordinate system, the origin is at the vertex O of H.G. and the x-axis is the grating normal. In the figure, C and D are the coherent point sources of wavelength λ_r. We consider a ray which originates from the center A of the entrance slit and is diffracted at point $P(\xi,w,1)$ on the nth groove of H.G., where the zeroth groove is the one passing through the vertex of H.G. The diffracted ray of wavelength λ in the mth order intersects the flat image plane L at point B. For the incident principal ray AO, the diffracted principal ray of λ in the mth order intersects L at point B_0. We assume for practical reasons that A, B_0, C, and D are located in the xy plane, and the polar coordinates of these points are (r_a,α), (r_b,β), (r_c,γ), and (r_d,δ), respectively.

For the ray APB, the light path function F is expressed as

$$\begin{aligned} F &= AP + PB_0 + nm\lambda \\ &= r_a+r_b+(w^2/2)F_{20}+(l^2/2)F_{02}+(w^3/2)F_{30}+(wl^2/2)F_{12}+ \ldots , \end{aligned} \tag{1}$$

where

$$F_{ij} = M_{ij}(r_a/R,r_b/R,\alpha,\beta) + (m\lambda/\lambda_r)H_{ij}(r_c/R,r_d/R,\gamma,\delta) , \tag{2}$$

$$\sin\alpha + \sin\beta = m\lambda/\sigma , \tag{3}$$

and σ, the effective grating constant, is expressed as

$$\sigma = \lambda_r/(\sin\delta - \sin\gamma) . \tag{4}$$

M_{ij} is determined from the mounting of the spectrograph, whereas H_{ij} is determined from the recording arrangement. Their explicit expressions are

found in ref. 15.

According to Fermat's principal, the stigmatic condition is expressed as

$$(\partial F/\partial w) = 0 \text{ and } (\partial F/\partial l) = 0 \text{ regardless of values of } w, l, \text{ and } \lambda. \quad (5)$$

It is, however, almost impossible to satisfy Eq.(5). Thus, for practical applications, it is sufficient to make

$$(\partial F/\partial w)^2 = \text{min. and } (\partial F/\partial l)^2 = \text{min.}$$
$$\text{for } |w| \leq w_0, \ |l| \leq l_0, \text{ and } \lambda_1 \leq \lambda \leq \lambda_2 \quad (6)$$

where $2w_0$ and $2l_0$ are the width and the hight of the grating respectively, and λ_1 and λ_2 are the shortest and longest wavelength to be measured respectively. Furthermore, condition (6) is approximately satisfied by minimizing certain low order expansion coefficients in Eq. (1).

Then, first-order mounting parameters are obtained from the following conditions where integration regions are same as shown in condition (6):

$$I_{20} = \int (F_{20})^2 \, d\lambda = \text{min.}, \quad (7)$$

and the condition for flat-field,

$$r_b = s/(\sin \beta - t \cos \beta) \ . \quad (8)$$

The recording parameters of H.G. are determined from Eqs. (4) and (7) and

$$I_{30} = \int (F_{30})^2 \, d\lambda = \text{min.}, \quad I_{12} = \int (F_{12})^2 \, d\lambda = \text{min.} \quad (9)$$

It should be noted that Eqs. (4), (7), (8), and (9) do not guarantee to give a realizable solution for the recording parameters, especially for grazing incidence arrangement. If this is the case, the design conditions should be loosened until a practical solution is obtained.

The optimum flat image-plane L is determined by tracing rays through the system for wavelengths under consideration and by minimizing the merit function

$$V = \int Q(\int \Delta b(\lambda)^2 dwdl)d\lambda \ , \quad (10)$$

where Q is a weight function, Δb is the distance between the points B and B_0. In the actual calculation, this integration is approximated by summation over a certain number of wavelengths.

3.2 Designed constants

In Eqs. (7) and (8), the wavelength region λ_1-λ_2 and the incident angle α are already given from the considerations mentioned in Sec. 2, thus the mounting parameters to be determined are r_a, r_b, ϕ, and σ. We solved Eqs. (7) and (8) by fixing σ, which is determined from the position r_b and the length l of the image plane. A range of 200-300 mm is chosen for r_b, and a range of l to match the detector is 20-50 mm, thus the groove number of 300 g/mm is expected to give a practical solution for S3. For other spectrographs, the groove number is also determined by the relation of r_b and l. The adopted values are 1200 g/mm for S1, and 300 g/mm for S2 and S4. With these conditions, the solutions of r_a, r_b, and ϕ which satisfy Eqs. (7) and (8) are computed. The results for S3 and S4 are shown in Fig. 4.

The relation of r_a and r_b, normalized by R cosα, is almost the same for S3 and S4. This enables us to design similar grazing incidence type spectrographs. From this figure, the solution, where r_a and r_b are nearly equal and ϕ is less than 35°, is selected as an approximate solution.

In the second step, Q is changed according with λ. For wavelength region longer than 5 nm, Δb changes moderately and we set Q as 1. For the shorter wavelength region, Δb changes sharply and Q is set as 5.

The instrumental constants of four spectrographs caluculated by the above method are shown in Table 1. The value of r_a, 238 mm, is made common for all spectrographs. Distance from the entrance slit to image plane is within 500 mm. The resultant value of ϕ is within 30° and the length of image plane l is within 40 mm. These values satisfy the requirements for JT-60 plasma diagnosis.

The inverse linear dispersion ($d\lambda/dl$) for m = 1 is given by following equation,

$$d\lambda/dl = \sigma \cos\beta \cos\phi/r_b \ . \qquad (11)$$

For S3, the values of ($d\lambda/dl$) are 0.5 nm/mm at λ = 0.5 nm, and 2.4 nm/mm at 50 nm. The grating constant varies across the grating surface gradually. The case of the grating for S3 is shown in Fig. 5.

3.3 Line profile and wavelength resolution

For all the spectrographs designed here, line profiles of spectral images with a point source and an entrance slit size of 50 μm(w) × 5 mm(h) are computed. Line profiles of S2 with the entrance slit are shown in Fig. 6, where the size of the grating is assumed 36 mm(w) × 5 mm(h).

These spectrographs show charactristic line profiles that are steep on the long wavelength side and slow on the short side. This is due to the residual coma type aberration. This asymmetric profile appears in the longer wavelength region and the widening of the profile by defocus appears in the shorter wavelength region. These aberrations are well corrected only in narrow wavelength region, for example, around 1 nm for S2. However, full width of the profile is nearly within 100 μm, and in most cases FWHM of 30-40 μm, smaller than the slit width, is expected.

The ratio of stigmatic image width a_i to the entrance slit width a_s is shown in Fig. 7, which is given by

$$a_i/a_s = r_b \cos\alpha/r_a \cos\beta \cos\phi \ . \tag{12}$$

It is 0.6 at 1 nm and 0.2 at 20 nm for S2, for example. Thus, narrower FWHM values than a_s are obtained.

From Fig. 6 and similar calculations for other spectrographs, FWHM of 30-40 μm is expected over the required wavelength region, except for wavelengths shorter than 1 nm in the case of S2. The resolution ($\lambda/d\lambda$) corresponding to 35 μm on image plane is shown in Fig. 8, and this satisfies the resolution requirement.

For the spectrographs with a photo-electric detector, the wavelength resolution is restricted by the detector resolution and the inverse linear dispersion of the spectrographs. When we assume the over all resolution of 50 μm on the image plane, $\lambda/d\lambda$ decreases to 70% of those shown in Fig. 8. The values of $\lambda/d\lambda$ of S1 are still better than the reference data of the JFT-2 experiment, and of S2 and S3 are comparable. Thus, these spectrographs with an entrance slit of 50 μm and a photo-electric detector satisfy the resolution requirement described in Sec. 1.

3.4 Spatial resolution

Spatial resolutions of the spectrographs in JT-60 plasma measurements are calculated from the geometric relations between the plasma and the spectrograph. We assume two apertures a_1 and a_2 in the spectrograph, where a_1 is the slit and a_2 is the grating or the detector. The distance of a_1 and a_2 and the distance of a_1 and the plasma are r and L_p, respectively, and the full width of the viewing field in the plasma is named a_w. Then a_w is given by

$$a_w = a_1 + (a_1 + a_2)\, L_p/r \ . \tag{13}$$

For the arrangement shown in Fig. 2, L_p is common for four spectrographs and 5175 mm. In the meridional plane of the spectrograph S1, that is, in the horizontal plane in this case, a_1 = 50 μm is the width of the entrance slit and a_2 = 0.63 mm is the aperture determined by the grating, and $r = r_a$ = 238 mm. Then a_w = 15 mm, and this value is smaller than the required spatial resolution of 70 mm. In the saggital plane, that is, in the vertical plane, a_1 = 5 mm is the hight of the entrance slit, a_2 = 2.5 mm is the detector hight, and $r = r_a + r_b$(min.) = 481 mm. Here, the value of a_1 is chosen tentatively, and the change of the direction of rays on the grating is neglected because of the grazing incidence arrangement. From Eq. (13), a_w = 86 mm is obtained, and exceeds 70 mm.

Now we consider the case where the a_w is smaller than 70 mm. From Eq. (13), the value a_1 which corresponds to a_w = 70 mm is 3.7 mm. In view of the light throughput, the larger value of the slit hight is desirable. A possible compromise is addition of one more aperture at the crossing point of the optical axes of the moduled spectrographs (see Fig. 2). This point is 3030 mm apart from the plasma center. If we choose the aperture of 29 mm in hight, a_w is 66 mm and satisfies the required resolution, and the corresponding entrance slit height is 7.4 mm. This means that twice the throughput can be obtained with additional aperture for the same spatial resolution of 70 mm. For other spectrographs, the values a_w in horizontal plane are 15 mm for S2, 28 mm for S3, and 69 mm for S4, and almost equal to that for S1 in vertical plane. Thus all spectrographs satisfy the required spatial resolution.

3.5 Light throughput

To calculate the light throughput of the spectrographs, we refer to Fig. 9. Here, I_p is the photon number per unit volume emitted from the plasma into all directions, b_p is the plasma length, a_s and H_s are the width and height of the entrance slit, F_m and F_s are F-numbers in the meridional and the saggital plane respectively, K_g is the grating efficiency, a_d and H_d are the width and height of the detector pixel respectively, and a_i and H_i are the width and height of the image respectively. The photon number N1 introduced into the spectrograph through the entrance slit is given by

$$N1 = I_p b_p a_s H_s / 4\pi F_m F_s \quad . \tag{14}$$

The photon number N2 fell into the detector pixel is given by

$$N2 = N1K_g \tag{15}$$

if the image is smaller than the pixel, and

$$N2 = N1K_g a_d H_d M_m M_s / a_i H_i \tag{16}$$

if the image is larger than the pixel, where M_m and M_s are the coefficients considering the intensity distribution of the image. With these equations, we can estimate the over all ratio $N2/I_p$. The values adopted for this calculation in the case of S1 is listed in Table 2.

At the center of the plasma, the plasma length is 180 cm. Considering the distribution of the photon number across the plasma area, we assumed the effective length as one-third the whole length. H_s is determined from the discussion on the spatial resolution. F_m is determined from the spectrogrph, but F_s is limited by the aperture between the plasma and the spectrograph. K_g is estimated as 2% from ref. 16. M_m is determined from the designed line profile and the detector width. Assuming the line profile is triangular with the bottom width a_i of 100 μm, and the pixel width a_d is 25 μm, M_m is 1.75 for the pixel at the center of the image. M_s is determined from the trapezoidal intensity distribution. With these values, $N2/I_p$ is calculated as 1.7×10^{-9} (cm^3) from Eqs. (14) and (16). Thus, for an I_p value of 1×10^{13} ($cps.cm^{-3}$), N2 is 1.7×10^4 (cps). Considering the integration time of 20 ms, we obtain 340 as the expected photon number per detector pixel. For other spectrographs, the values $N2/I_p$ is similar for S2, nearly twice for S3, and five times for S4, respectively, according the change of the incident angles. These are acceptable values for the detector.

4. Imaging properties with photographic plate

The imaging properties of the modularized spectrographs are examined with Kodak SWR photographic plate, and the wavelength resolution are checked in the wide wavelength region. The conditions of some examinations are listed in Table 3.

To examine the imaging properties in wavelength region shorter than 10 nm, a windowless Al target SX light source is prepared. The condition of the experiment for the spectrograph S2 is listed in Table 3-a, and the

The photon number N2 fell into the detector pixel is given by

$$N2 = N1K_g \tag{15}$$

if the image is smaller than the pixel, and

$$N2 = N1K_g a_d H_d M_m M_s / a_i H_i \tag{16}$$

if the image is larger than the pixel, where M_m and M_s are the coefficients considering the intensity distribution of the image. With these equations, we can estimate the over all ratio $N2/I_p$. The values adopted for this calculation in the case of S1 is listed in Table 2.

At the center of the plasma, the plasma length is 180 cm. Considering the distribution of the photon number across the plasma area, we assumed the effective length as one-third the whole length. H_s is determined from the discussion on the spatial resolution. F_m is determined from the spectrogrph, but F_s is limited by the aperture between the plasma and the spectrograph. K_g is estimated as 2% from ref. 16. M_m is determined from the designed line profile and the detector width. Assuming the line profile is triangular with the bottom width a_i of 100 μm, and the pixel width a_d is 25 μm, M_m is 1.75 for the pixel at the center of the image. M_s is determined from the trapezoidal intensity distribution. With these values, $N2/I_p$ is calculated as 1.7×10^{-9} (cm^3) from Eqs. (14) and (16). Thus, for an I_p value of 1×10^{13} ($cps.cm^{-3}$), N2 is 1.7×10^4 (cps). Considering the integration time of 20 ms, we obtain 340 as the expected photon number per detector pixel. For other spectrographs, the values $N2/I_p$ is similar for S2, nearly twice for S3, and five times for S4, respectively, according the change of the incident angles. These are acceptable values for the detector.

4. Imaging properties with photographic plate

The imaging properties of the modularized spectrographs are examined with Kodak SWR photographic plate, and the wavelength resolution are checked in the wide wavelength region. The conditions of some examinations are listed in Table 3.

To examine the imaging properties in wavelength region shorter than 10 nm, a windowless Al target SX light source is prepared. The condition of the experiment for the spectrograph S2 is listed in Table 3-a, and the

densitometer trace is shown in Fig. 10-a. Specular light is cut with filter, and stray light level is low enough. Al Kα line, λ = 0.83 nm, its higher order spectra, and other impurity lines, for example, O_2 (2.37 nm) and C (4.4 nm) are recorded. 1st order of Al Kα line is broadened because of the residual defocus around this wavelength region, while the 2nd order spectrum is quite narrow. The FWHM of the 1st order of Al Kα is 70 μm, which corresponds to dλ of 0.03 nm and λ/dλ is 30. The enlarged trace of the 2nd order of Al Kα is shown in Fig. 10-b. The FWHM of this profile is 20 μm, which corresponds to dλ of 0.01 nm and λ/dλ of 170 is obtained. The Al Kα line is also recorded with the spectrograph S1. The FWHM of the 1st order is 65 μm, dλ is 0.01 nm, and λ/dλ of 75 is obtained.

For the test in the wavelength region of 10-50 nm, an Al spark discharge light source was used. The conditions of the experiment for the spectrograph S3 are shown in Table 3-b, and the densitometer trace is shown in Fig. 11. A difference in dark level near 2 nm region shows stray light level. Spectra longer than 10 nm are recorded, and FWHM of 20-30 μm on photographic plate is attained in whole wavelength region. The smaller FWHM value of the experiment than the designed one is seemed that the narrower grating surface is exposed by the light source. The experiment with two He spectra, 30.4 nm and 58.4 nm, are also examined. The profiles are agree with the deisgned ones, and full width of 90 μm and FWHM of 30-40 μm are obtained for both spectra with a slit of 50 μm. The resolution λ/dλ corresponds to 35 μm on the photographic plate is 230 at 10 nm, 450 at 30 nm and 600 at 50 nm.

In the wavelength region longer than 50 nm, a continuous discharge light source with He gas was used. The condition of the experiment for the spectrograph S4 is shown in Table 3-c. Flat field property is also realized and spectra are well resolved in whole wavelength region. Densitometer traces at 66 nm and 115 nm are shown in Fig. 12. Spectra with FWHM of 20 μm are obtained with a slit of 20 μm, and the caluculated resolution λ/dλ for two wavelengths are 1000 at 66 nm and 1500 at 115 nm.

These results show that the produced gratings and spectrographs satisfy the designed imaging properties and are suitable for coupling with photo-electric detector for JT-60 plasma diagnosis.

5. Conclusion

New modularized flat field grazing incidence spectrographs which cover wide wavelength region down to 0.5 nm and have appreciable resolving power are designed. The designed characteristics are summarized, and the optical design and optical performance are discussed in detail. The preliminary tests with photographic plates are examined, and Al Kα (0.83 nm), Al discharge spectra in 10-50 nm, and He spectra in 30-120 nm are recorded. These spectrographs show the designed flat-field properties and wavelength resolution in whole wavelength region.

The main features of the modularized spectrographs are:

(1) time- and space-resolved spectrographs for the wavelength region 0.5-122 nm are realized,
(2) handling of the spectrographs is easy, and needs no skill,
(3) the measurement in a wide wavelength region is possible using an array detector having a total width of 25 mm or 50 mm,
(4) the compact spectrographs with the same size and the positions of the components are almost same can be produced,
(5) spectrographs are designed with holographic gratings, and it makes easy to realize other spectrographs, for example, with higher resolution in a specified narrow wavelength region.

The modularized spectrographs are suitable for large TOKAMAK (JT-60) plasma diagnosis as described above, and are also available for other spectroscopic measurements in soft X-ray and VUV wavelength region.

Acknowledgment

This work has been done as a part of the construction program of an impurity measurement system for JT-60 TOKAMAK plasmas. We would like to express our thanks to Drs. Y. Suzuki, H. Maeda, and H. Kubo of Japan Atomic Energy Research Institute, Messrs. J. Morimoto, M. Tsuchiya, M. Noguchi, and F. Urakawa of Nikon for their valuable discussions on these spectrographs. We are indebted to Messrs. N. Kihara, M. Hagiwara, and Y. Imai of Nikon for their successful assistant on the test of imaging properties. We are also indebted to Prof. T. Namioka of Tohoku Univ., Messrs. S. Yoshida and N. Shiotake of Nikon for their encouragement throughout the present work. And the continuing support of Drs. S. Mori, M. Yoshikawa, S. Tamura, T. Iijima, and A. Funahashi of Japan Atomic Energy Research Institute is gratefully acknowledged.

5. Conclusion

New modularized flat field grazing incidence spectrographs which cover wide wavelength region down to 0.5 nm and have appreciable resolving power are designed. The designed characteristics are summarized, and the optical design and optical performance are discussed in detail. The preliminary tests with photographic plates are examined, and Al Kα (0.83 nm), Al discharge spectra in 10-50 nm, and He spectra in 30-120 nm are recorded. These spectrographs show the designed flat-field properties and wavelength resolution in whole wavelength region.

The main features of the modularized spectrographs are:

(1) time- and space-resolved spectrographs for the wavelength region 0.5-122 nm are realized,
(2) handling of the spectrographs is easy, and needs no skill,
(3) the measurement in a wide wavelength region is possible using an array detector having a total width of 25 mm or 50 mm,
(4) the compact spectrographs with the same size and the positions of the components are almost same can be produced,
(5) spectrographs are designed with holographic gratings, and it makes easy to realize other spectrographs, for example, with higher resolution in a specified narrow wavelength region.

The modularized spectrographs are suitable for large TOKAMAK (JT-60) plasma diagnosis as described above, and are also available for other spectroscopic measurements in soft X-ray and VUV wavelength region.

Acknowledgment

This work has been done as a part of the construction program of an impurity measurement system for JT-60 TOKAMAK plasmas. We would like to express our thanks to Drs. Y. Suzuki, H. Maeda, and H. Kubo of Japan Atomic Energy Research Institute, Messrs. J. Morimoto, M. Tsuchiya, M. Noguchi, and F. Urakawa of Nikon for their valuable discussions on these spectrographs. We are indebted to Messrs. N. Kihara, M. Hagiwara, and Y. Imai of Nikon for their successful assistant on the test of imaging properties. We are also indebted to Prof. T. Namioka of Tohoku Univ., Messrs. S. Yoshida and N. Shiotake of Nikon for their encouragement throughout the present work. And the continuing support of Drs. S. Mori, M. Yoshikawa, S. Tamura, T. Iijima, and A. Funahashi of Japan Atomic Energy Research Institute is gratefully acknowledged.

References

1. T. Namioka, H. Noda, and M. Seya, "Performance of aberration-reduced holographic concave gratings designed specifically for Seya-Namioka monochromators" J. Spectrosc. Soc. Jpn., 23, suppl. 1, 29 (1974)
2. D. Lepere, "Monochromateur a simple rotation du reseau, reseau holographique sur support torique pour l'ultraviolet lointain" Mouv. Rev. Opt., 6, 173 (1975)
3. T. Harada and T. Kita, "Mechanically ruled aberration-corrected concave gratings" Appl. Opt., 19, 3987 (1980)
4. J. Flamand, G. Passereau, A. Thevenon, and J.M. Lerner, "Performance analysis of toroidal grating flat field spectrographs for use in the far UV" Ext. Abstr. VIth Intern. Conf. Vacuum UV Radiation Phys. III, III-21 (Charlottesville, 1980)
5. T. Aton, C. Franck, E. Kallne, S. Schnatterly, and F. Zutavern, "A new toroidal grating spectrometer for the soft X-ray region" Nucl. Instrum. Methods, 172, 173 (1980)
6. R.J. Fonck, A.T. Ramsey, and R.V. Yell, "Multichannel grazing-incidence spectrometer for plasma impurity diagnosis: SPRED" Appl. Opt., 21, 2115 (1982)
7. T. Kita, T. Harada, N. Nakano, and H. Kuroda, "Mechanically ruled aberration-corrected concave gratings for a flat-field grazing-incidence spectrograph" Appl. Opt., 22, 512 (1983)
8. N. Nakano, H. Kuroda, T. Kita, and T. Harada, "Development of a flat-field grazing-incidence XUV spectrometer and its application in picosecond XUV spectroscopy" Appl. Opt., 23, 2386 (1984)
9. B.C. Stratton, R.J. Fonck, K. Ida, K.P. Jaehnig, and A.T. Ramsey, "SPRED spectrograph upgrade: High-resolution grating and improved absolute calibrations" Rev. Sci. Instrum., 57, 2043 (1986)
10. T. Hirayama, T. Sugie, A. Sasaki, H. Kubo, Y. Koide, N. Akaoka, H. Takeuchi, and M. Nagai, "Impurity Transport in Ohmically Heated JT-60 Plasma" JAERI-M 86-161 (1986)
11. JT-60 Team, "Review of Preliminary Additional Heating Experiments in JT-60 (Aug. -Nov., 1986)" JAERI-M 87-009, 166 (1987) (in Japanese)
12. T. Sugie, H. Kubo, A. Sasaki, Y. Koide, N. Nishino, N. Akaoka, and H. Takeuchi, "Spectroscopic System for Spatially Resolved Impurity Measurement on JT-60" KAKUYUGO KENKYU, 59, supplement, 157 (1988) (in Japanese)

13. B.L. Henke, P. Lee, T.J. Tanaka, R.L. Shimabukuro, and B.K. Fujikawa, "Low-energy X-ray interaction coefficients: photoabsorption, scattering, and reflection" Atomic Data and Nuclear Data Tables 27, 1 (1982)
14. W.R. Hunter and D.W. Angel "Optical properties of evaporated platinum films in the vacuum ultraviolet from 2200 A to 150 A" J. Opt. Soc. Am., 69, 1695 (1979)
15. H. Noda, T. Namioka, and M. Seya, "Geometric theory of the grating" J. Opt. Soc. Amer., 64, 1031 (1974)
16. R.J. Speer, "A comparative review of grazing incidence gratings, including recent measurements on the performance of stigamatic soft X-ray reflection gratings formed holographically" J. Spectrosc. Soc. Jpn., 23, suppl. 1, 53 (1974)

Table 1 Constants of four spectrographs.

	S1	S2	S3	S4
wavelength region	0.5-5nm	0.5-50nm	2-50nm	50-122nm
α	89°	89°	88°	85°
σ	1/1200mm	1/300mm	1/300mm	1/300mm
r_a	238mm	238mm	238mm	238mm
r_b(max)	250mm	256mm	234mm	245mm
ϕ (max)	24°	15°	20°	15°
l	20mm	39mm	31mm	23mm

Table 2 Values for the light throughput estimation.

$I_p = 1 \times 10^{13}$ cps.cm^{-3}	$a_d = 25$ μm
$b_p = 60$ cm	$H_d = 2.5$ mm
$K_g = 0.02$	$a_i = 100$ μm
$a_s = 50$ μm	$H_i = 13.9$ mm
$H_s = 7.4$ mm	$M_m = 1.75$
$F_m = 380$	$M_s = 1.7$
$F_s = 74$	

Table 3 Conditions of the experiment with photographic plate.

experiment	a	b	c
module number	S2 (0.5-50nm)	S3 (2-50nm)	S4 (50-122nm)
light source			
electrode/gas	Al	Al	He
voltage	5Kv	10Kv	8Kv
shot number/current	1mA(cont.)	3shots/min.	100mA(cont.)
slit width of spectrograph	20μm	50μm	20μm
exposure time	90min.	50min.	20min.
development time D-19, twice thinned	4min.	4min.	4min.
slit width of densitometer	10μm	10μm	10μm

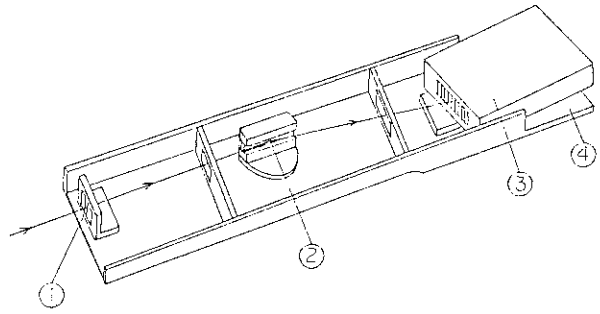

Fig. 1 Schematic diagram of the modularized spectrograph.
① entrance slit ② grating ③ detector ④ base plate.

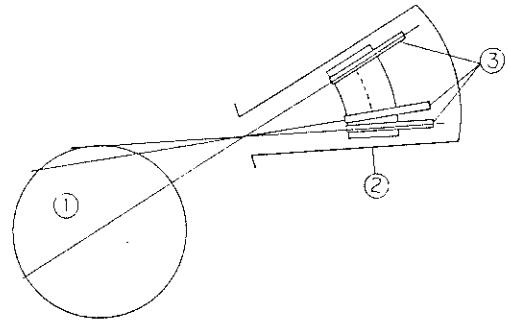

Fig. 2 Arrangement of the spectrographs for the space-resolved diagnosis of large TOKAMAK plasma. ① cross section of TOKAMAK plasma ② vacuum vessel with seventeen guide bars ③ modularized spectrographs.

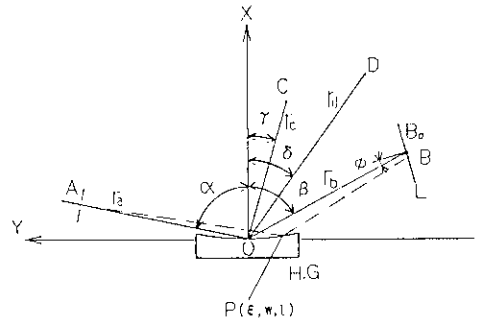

Fig. 3 Schematic diagram of grazing incidence flat-field spectrograph and recording system of holographic diffraction grating.

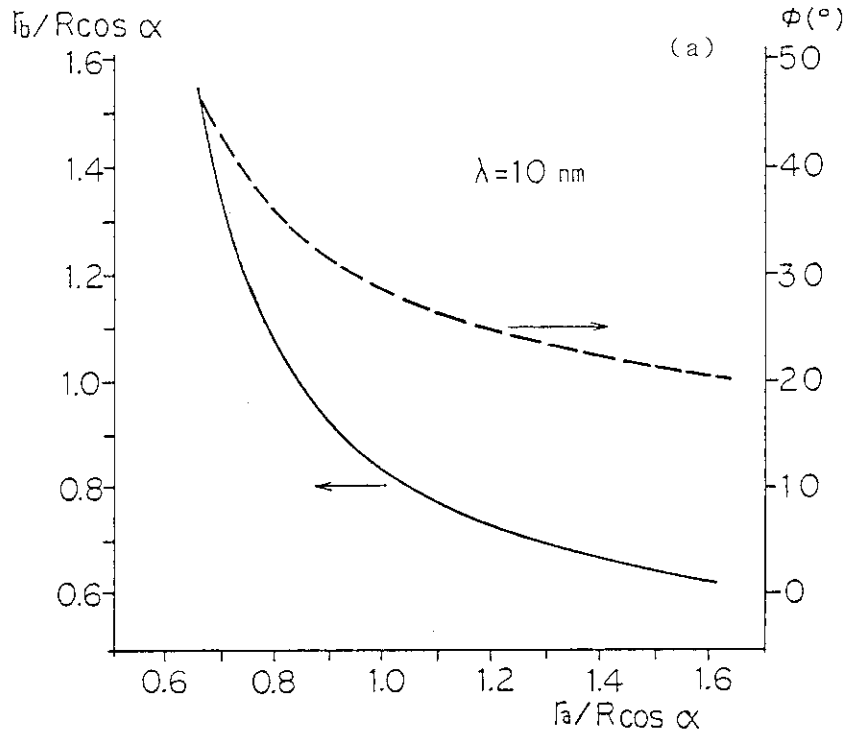

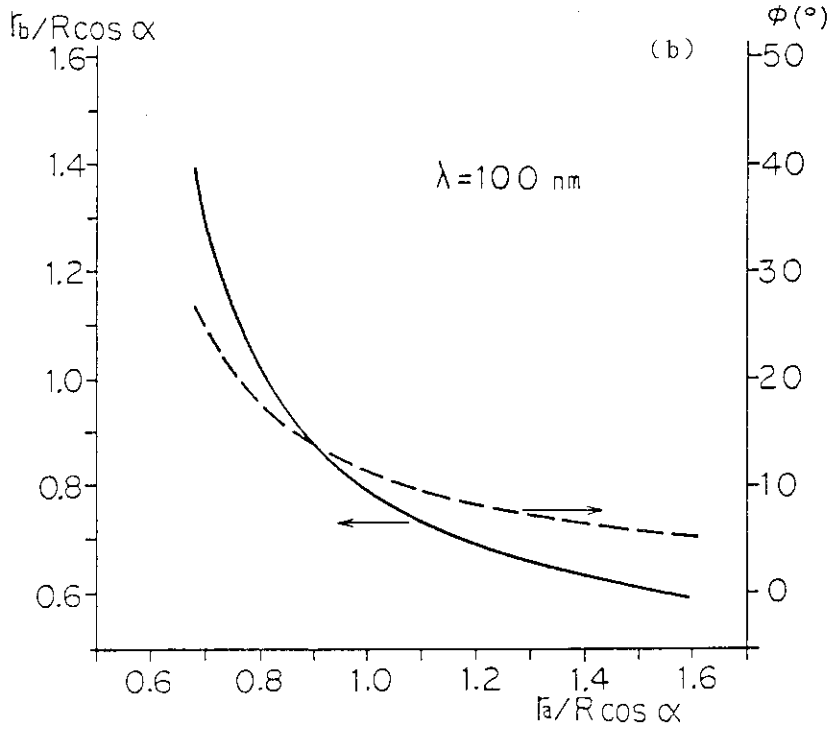

Fig. 4 Relation of r_a and r_b, r_a and ϕ which satisfies conditions for an approximate solution, (a) at 10nm for S3, and (b) at 100nm for S4.

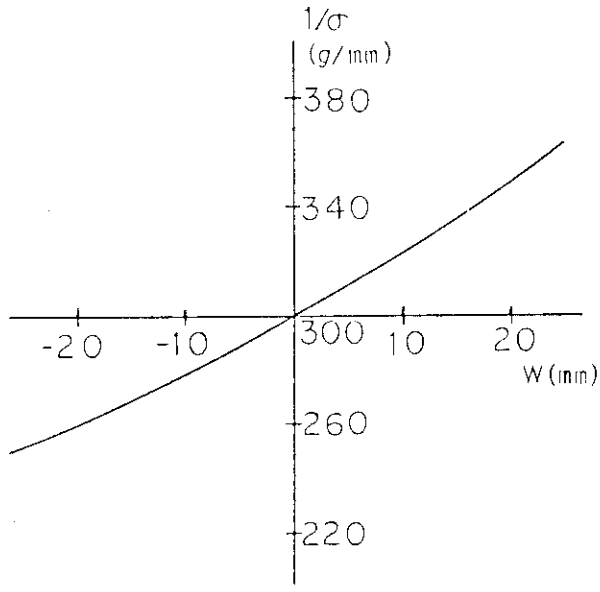

Fig. 5 Change of grating constant on a grating for S3.

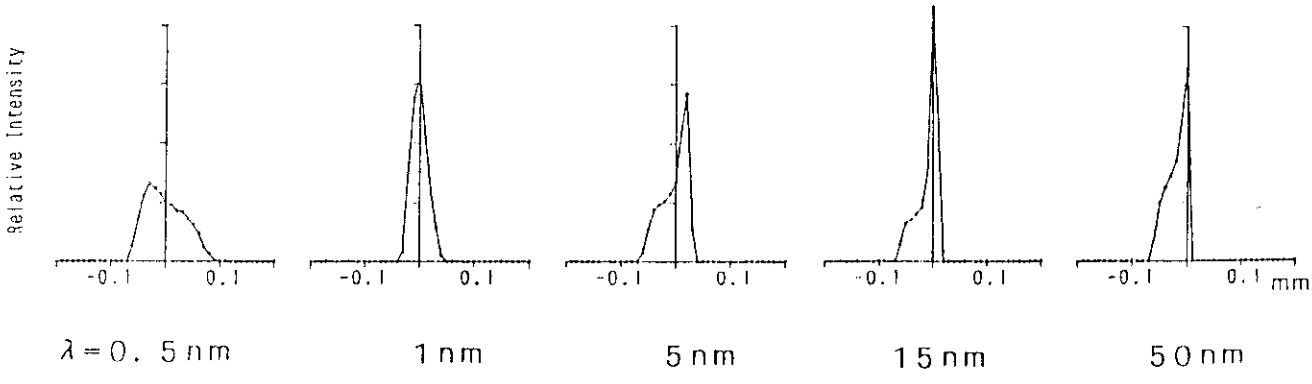

Fig. 6 Designed line profile for S2 with an entrance slit of 50 μm.

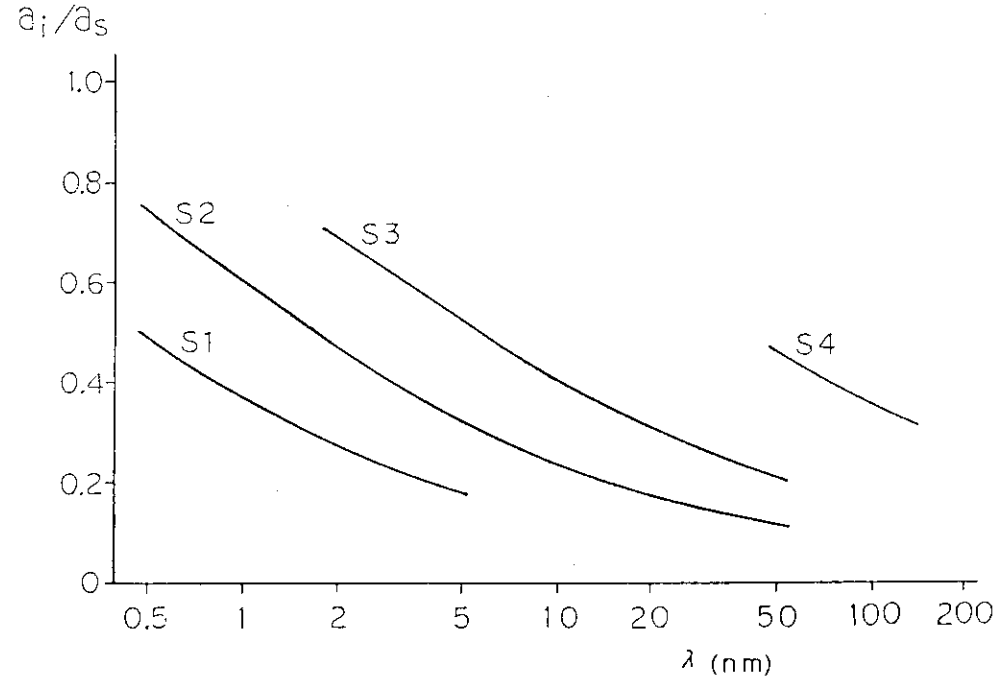

Fig. 7 Ratio of stigmatic image width a_i to entrance slit width a_s.

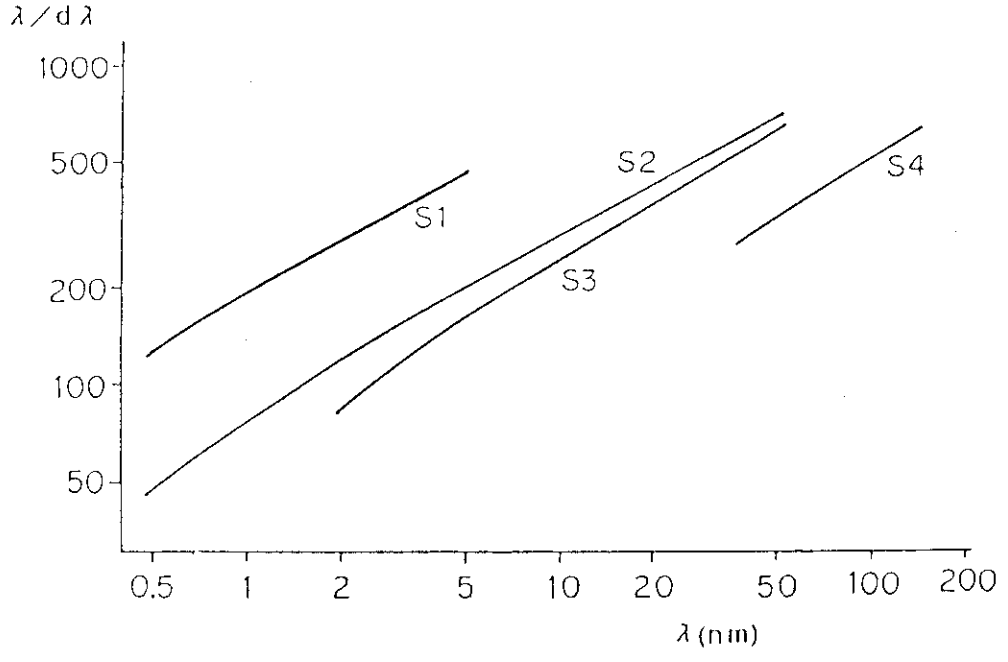

Fig. 8 Spectral resolution λ/dλ corresponds to 35 μm on image plane.

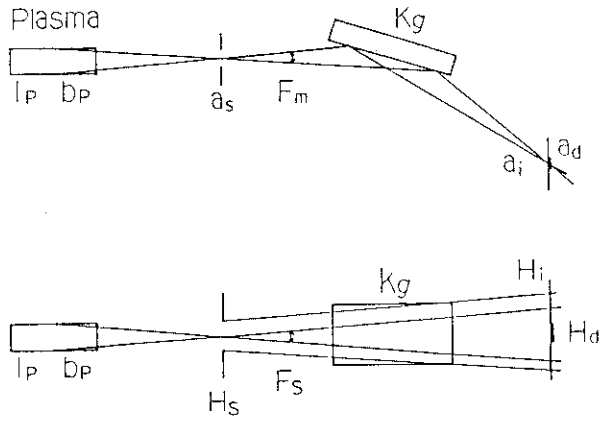

Fig. 9 Schmatic diagram for the calculation of light throughput, (a) in the meridional plane and (b) in the saggital plane.

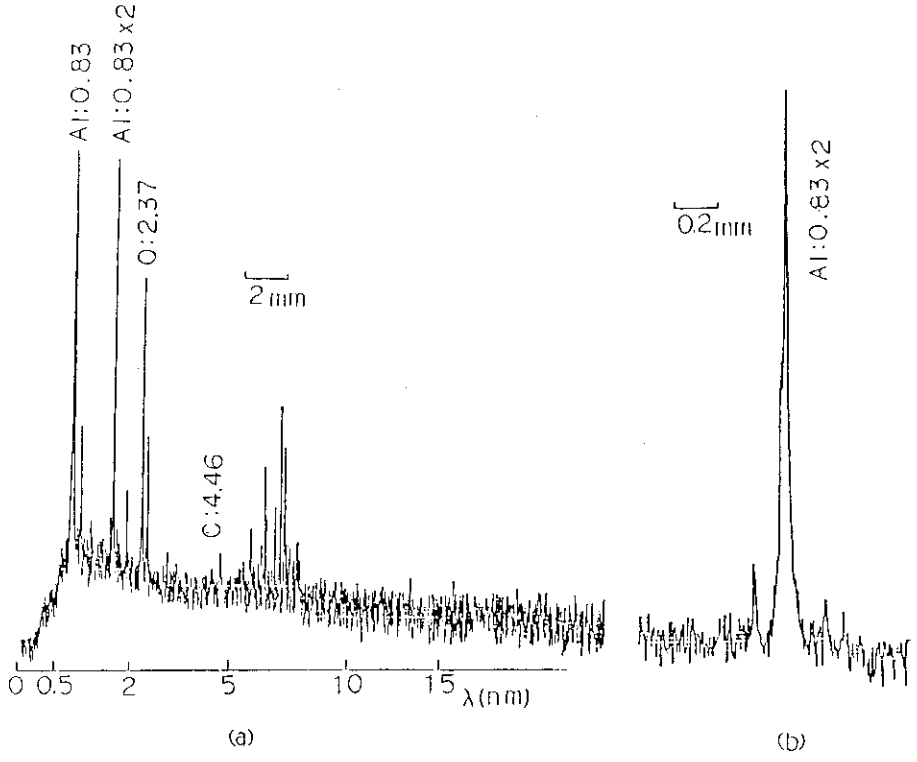

Fig. 10 Densitometer trace of the photographic plate taken with the spectrograph S2 and Al-target SX light source. (a) wavelength region of 0.5-15 nm, and (b) enlarged trace at 1.7nm. The condition of the experiment is listed in Table 3-a.

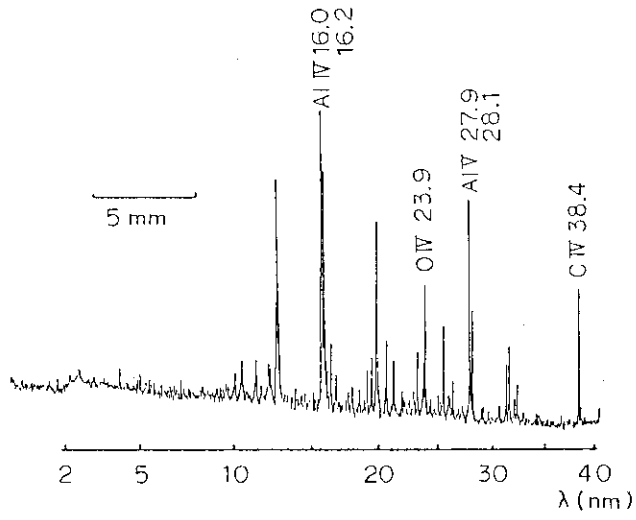

Fig. 11 Densitometer trace of the photographic plate taken with the spectrograph S3 and Al spark discharge light source. The condition of the experiment is listed in Table 3-b.

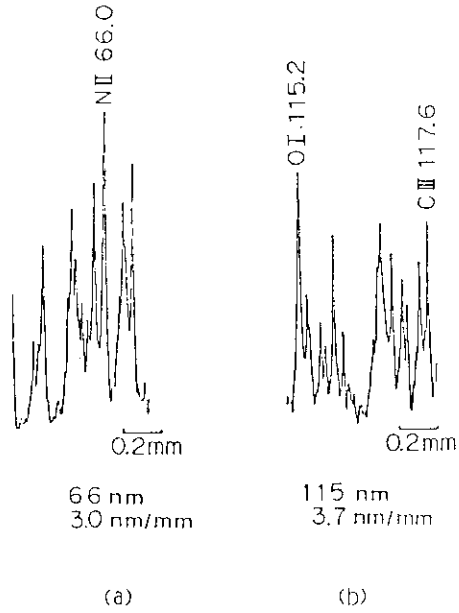

Fig. 12 Densitometer trace of the photographic plate taken with the spectrograph S4 and He gas discharge light source at (a) 66nm and (b) 115nm. The condition of the experiment is listed in Table 3-c.